



## Hyperfine-Resolution Mapping of On-Road Vehicle Emissions with Comprehensive Traffic Monitoring and Intelligent Transportation System

5 Linhui Jiang<sup>1</sup>, Yan Xia<sup>1</sup>, Lu Wang<sup>1</sup>, Xue Chen<sup>1</sup>, Jianjie Ye<sup>5</sup>, Tangyan Hou<sup>1</sup>, Liqiang Wang<sup>1</sup>, Yibo Zhang<sup>1</sup>,  
Mengying Li<sup>1</sup>, Zhen Li<sup>1</sup>, Zhe Song<sup>1</sup>, Yaping Jiang<sup>1</sup>, Weiping Liu<sup>1</sup>, Pengfei Li<sup>3+</sup>, Daniel Rosenfeld<sup>4</sup>, John  
H. Seinfeld<sup>2</sup>, Shaocai Yu<sup>1,2+</sup>

<sup>1</sup>Research Center for Air Pollution and Health; Key Laboratory of Environmental Remediation and Ecological Health, Ministry of Education, College of Environment and Resource Sciences, Zhejiang University, Hangzhou, Zhejiang 310058, P.R. China

10 <sup>2</sup>Division of Chemistry and Chemical Engineering, California Institute of Technology, Pasadena, CA 91125, USA.

<sup>3</sup>College of Science and Technology, Hebei Agricultural University, Baoding, Hebei 071000, P.R. China

<sup>4</sup>Institute of Earth Sciences, The Hebrew University of Jerusalem, Jerusalem, Israel

<sup>5</sup>Bytedance Inc., Hangzhou, Zhejiang 310058, China

15 <sup>+</sup>Correspondence to: Shaocai Yu (shaocaiyu@zju.edu.cn); Pengfei Li (lpf\_zju@163.com)

20

25



## 30 Abstract

Urban on-road vehicle emissions affect air quality and human health locally and globally. Such emissions typically exhibit distinct spatial heterogeneity, varying sharply over short distances (10 m ~ 1km). However, all-around observational constraints on the emission sources are limited in much of the world. Consequently, traditional emission inventories lack the spatial resolution that can characterize on-road  
35 vehicle emission hotspots. Here we establish a bottom-up approach to reveal a unique pattern of urban on-road vehicle emissions at 1 ~ 3 orders of magnitude higher spatial resolution than current inventories. We interconnect all-around traffic monitoring (including traffic fluxes, vehicle-specific categories, and speeds) via an intelligent transportation system (ITS) over the Xiaoshan District in the Yangtze River Delta (YRD) region. This enables us to calculate single-vehicle-specific emissions over each fine-scale  
40 (10 m ~ 1 km) road segment. Thus, a hyperfine emission dataset is achieved, and on-road emission hotspots appear. The resulting map shows that the hourly average on-road vehicle emissions of CO, NO<sub>x</sub>, HC, and PM<sub>2.5</sub> are 74.01 kg, 40.35 kg, 8.13 kg, and 1.68 kg, respectively. More importantly, widespread and persistent emission hotspots emerge, of significantly sharp small-scale variability, up to 8 ~ 15 times, attributable to distinct traffic fluxes, road conditions, and vehicle categories. On this basis, we investigate  
45 the effectiveness of routine traffic control strategies on on-road vehicle emission mitigation. Our results have important implications for how the strategies should be designed and optimized. Integrating our traffic-monitoring-based approach with urban air quality measurements, we could address major data gaps between urban air pollutant emissions and concentrations.



## 1. Introduction

50 Rapid growth in vehicle population for decades has led to widespread and severe levels of fine particulate matter (PM<sub>2.5</sub>) and ozone (O<sub>3</sub>) (Anenberg et al., 2017; He et al., 2020; Huang et al., 2020; Kelly and Zhu, 2016; Tessum et al., 2014; Zhang et al., 2012, 2019). However, the gradients of on-road vehicle emissions are not well represented in routine emission inventories. That is, the traffic states (e.g., traffic fluxes, road conditions, and vehicle categories) can vary sharply over short distances (10 m ~ 1  
55 km), particularly in urban zones (Chen et al., 2020; Gately et al., 2017; Liu et al., 2019; Wu et al., 2019; Yu et al., 2020). Routine inventories of on-road vehicle emissions are established based on macro-scale and retrospective statistics. Consequently, they are temporally static for a historical year or month and spatially coarse (> 1 ~ 25 km) (Janssens-Maenhout et al., 2015; Li et al., 2017; Zhang et al., 2013). Earlier studies have applied traffic models to improve spatiotemporal resolution (Zhang et al., 2016). However,  
60 given that the traffic states were assumed, the simulated emissions were prone to deviate from real-world situations, especially from fine-scale gradients. More importantly, the emission hotspots and their anthropogenic drivers are missed.

Recently, significant advances have been made in comprehensive traffic monitoring techniques. These methods include GPS-instrumented floating cars (e.g., GPS-equipped probe taxis), open-access  
65 congestion maps, radio frequency identification, and traffic video records, each of which has distinct advantages and limitations (Gately et al., 2017; Gately and Hutyrá, 2017; Jing et al., 2016; Liu et al., 2018; Wen et al., 2020; Wu et al., 2019; Yang et al., 2019, 2018b). The individual GPS-instrumented floating cars allow us to extrapolate regional-scale vehicle activity levels. Yet, they are relatively scarce compared to the whole fleet, unable to characterize the fine-scale gradients (10m ~ 1km) as well as emission hotspots.  
70 Open-access congestion maps typically originate from navigation software, such as Baidu Map. Technically, they collect locations of individual mobile phones as real-time traffic information. On this basis, hierarchical traffic congestion indices can be built up and treated as spatiotemporal surrogates of traffic fluxes and speeds. Despite this, the information for individual vehicles, like speed and categories, remains unavailable. A recent study (Deng et al., 2020) utilized the BeiDou Navigation Satellite System  
75 to develop a full-sample high-resolution emission inventory, but only for trucks.



In contrast, comprehensive traffic monitoring technologies, such as radio frequency identification (Paul et al., 2013) coupled with traffic video records (Song et al., 2019), can offer valuable opportunities to obtain real-time vehicle-specific traffic information. Despite this, in the United States, daily traffic activities are released annually at the state-level rather than at high spatiotemporal resolution (hourly and  
80 10m ~ 1km) (Gately et al., 2013). On the other hand, those facilities are inter-complementary but usually owned and operated by different governmental agencies or private companies. Hence, relying on either party, hyperfine-resolution emission inventories cannot be derived comprehensively.

It is essential to introduce an intelligent transportation system (ITS) that is capable of interconnecting independent traffic monitoring and thus offering a complete picture of traffic states (Avila  
85 and Mezić, 2020; Yang et al., 2020; Zhang et al., 2018). Here, we derive a hyperfine-resolution on-road vehicle emission inventory. For most developing regions, especially in populous parts of Asia and Africa, such an integrated system is largely absent.

As one of the most developed regions in the Yangtze River Delta (YRD), the Xiaoshan District is confronting severe air pollution, particularly with surface O<sub>3</sub> frequently exceeding air quality standards  
90 in summertime (<http://www.cnemc.cn/>). Moreover, this is one of few areas, in which comprehensive traffic monitoring realizes full coverage and is interconnected via an ITS (named “City Brain”) since 2017 (Fig. 1) (Hua, 2018). This allows one to calculate single-vehicle-specific emissions over each fine-scale (10 m ~ 1 km) road segment. Consequently, here we derive the largest and most hyperfine urban on-road vehicle emission dataset of its type. Thus, fine-scale gradients (10 m ~ 1 km) and hotspots of on-road  
95 vehicle emissions are exposed. On this basis, we can directly evaluate the potential impacts of precise (e.g., vehicle-type-specific, road-segment-specific, or traffic-flux-specific) emission mitigation strategies. Our results provide new insights into the spatial variability of urban on-road vehicle emissions.

## 2. Materials and methods

The objective of this study is to apply a bottom-up model approach to establish a hyperfine-  
100 resolution inventory of on-road vehicle emissions over the Xiaoshan District in the YRD (Fig. 1). All key input data, including traffic fluxes, vehicle-specific categories, and vehicle speeds, were obtained from comprehensive traffic monitoring coupled with an ITS. Besides, vehicle-specific emission factors come



from the local official vehicle Inspect/Maintenance (I/M) dataset, the methodology of which has been described in China's National Emission Inventory Guidebook (ICCT, 2020).

## 105 2.1. Comprehensive traffic monitoring network

The Xiaoshan District, located in the YRD in China (Fig. 2) had in 2019 a population of over 1.58 million, 18.56% of the population of New York City. Its GDP was close to 200 billion Yuan, ranking fifth among districts in China. The total length of the road network was around 2000 km within a limited geographical extent (i.e., 1417.83 km<sup>2</sup>). With this background, the Xiaoshan District has become an important urban transportation hub in the YRD, for which on-road vehicle emissions were projected to be intensive and to play a critical role in affecting fine-scale air quality (and exposure equity). Since 2016, routine measures to ease traffic congestion, such as license restrictions during the morning and afternoon rush hours, were implemented over the Xiaoshan District. This would significantly alter fine-scale spatiotemporal patterns of traffic states (including traffic fluxes, vehicle speeds, and fleet compositions) and thus on-road vehicle emissions, the impacts of which remain unclear.

## 115 2.2. Hyperfine-resolution bottom-up model framework

A hyperfine-resolution bottom-up model framework was established to calculate primary on-road vehicle emissions, including carbon monoxide (CO), hydrocarbons (HC), nitrogen oxides (NO<sub>x</sub>), and PM<sub>2.5</sub>. Figure 1 is a flow diagram to illustrate the overall methodology for this framework. The results depend on an ensemble calculation of traffic fluxes, road segments, vehicle-specific speed, categories, and emission factors (Eq. 1) (Wu et al., 2019; Yang et al., 2019; Zhang et al., 2016):

$$E_{h,j,l} = \sum_t EF_{c,j}(v) \times TF_{c,h,l} \times L_l, \text{ (Eq. 1)}$$

$E_{h,j,l}$  is the consequent emission of the pollutant  $j$  on the road link  $l$  at the hour  $h$ , the unit of which is grams per hour (g h<sup>-1</sup>), while the remaining variables denote the input data for the model.  $EF_{c,j}(v)$  is the average emission factor of the pollutant  $j$  for the vehicle category  $c$  at the speed  $v$ , the unit of which is grams per kilometre (g km<sup>-1</sup>);  $TF_{c,h,l}$  is the traffic flux of the vehicle category  $c$  on the road segment  $l$  at the hour  $h$ , in units of vehicles per hour (veh h<sup>-1</sup>);  $L_l$  is the length of the road segment  $l$  in units of kilometres (km).



The major technical advance in this study is that all these input data were vehicle-specific and  
130 obtained from all-round traffic monitoring, introduced and detailed in Sect. 2.3. Detailed road segments  
are important carriers reflecting traffic states and on-road vehicle emissions. In this study, we divided the  
entire road network over the Xiaoshan District into 1894 road segments. Over the entire district, such  
road segments were divided into three road classes: highways, arterial roads, and residential streets (Fig.  
2). Spatially, each road segment was adaptive to a set of traffic monitoring platforms that can collect  
135 comprehensive traffic profiles, including traffic fluxes, vehicle-specific categories, and speeds. Therefore,  
the all-round traffic monitoring derived the hyperfine-resolution map of road segments and thus  $E_{h,j,l}$ .

To obtain the key input data for this model, we explored traffic monitoring information that  
achieved full coverage over the Xiaoshan District (Fig. 2). On this basis, vehicle-specific speed and  
categories were collected. Besides, the vehicle-category-specific emission factors were obtained from the  
140 local official I/M dataset. Consequently, an ITS (named “City Brain”) was developed to simultaneously  
upload the traffic monitoring information and, more importantly, to establish vehicle-specific links  
between those parameters. Therein, traffic fluxes played a major role in affecting vehicle emissions (Deng  
et al., 2020; Yang et al., 2019). Particularly, traffic congestion in narrow spaces might contribute to urban  
emission hotspots. To this end, traffic video records, together with image recognition algorithms, were  
145 applied to detect vehicle license plates and thus to monitor traffic fluxes. As a result, we constructed a  
total dataset of 254.31 million records from 13 November 2020 to 13 January 2021. Such measurements  
were recorded by different video facilities integrated into the ITS and thus accessible simultaneously.  
Moreover, accurate vehicle speeds are another key driver that is of great significance for optimizing  
vehicle emission factors (Yang et al., 2019). Here, together with traffic fluxes, the vehicle-specific speed  
150 was measured concurrently by radar velocimeters. Collectively, a high-resolution map of traffic states,  
including traffic fluxes and vehicle-specific speed, was captured by comprehensive traffic monitoring  
over the Xiaoshan District. From this perspective, this work is distinct from previous attempts that  
introduced spatial surrogates for traffic states (e.g., floating cars and traffic congestion index in open-  
source maps) to fill the monitoring gaps. Other key input data are the vehicle-specific category that is  
155 closely related to vehicle-specific emission factors (Huang et al., 2020). For each vehicle, an image  
detection technology based on traffic video records was utilized to recognize license plate and category.



According to the license plate, the identified vehicle category is verified via the I/M data. Herein, six vehicle categories were detected and defined, including light-duty vehicles (LDVs), middle-duty vehicles (MDVs), heavy-duty vehicles (HDVs), light-duty trucks (LDTs), middle-duty trucks (MDTs), and heavy-duty trucks (HDTs).  
160

According to the detected license plates, these vehicles fell into two types: registered vehicles and non-registered ones in the local official I/M dataset. The emission factors of the former were vehicle-category-specific and speed-dependent, obtained from the I/M dataset, while those of the latter were also speed-dependent but vehicle-category-specific averages (Fig. S1). Here, the detailed species profiles of HC, as well as evaporative HC, were not included.  
165

### 2.3. Traffic control strategies

Based on a hyperfine-resolution map of on-road vehicle emissions, the impacts of traffic control measures on vehicle emission reductions can be directly investigated. Here, four scenarios were designed, which were mainly oriented to traffic fluxes and fleet compositions. Therein the key point was to determine how to conduct these strategies spatially and temporally (Table 1). First, the routine scenario (S1) was conducted during the morning and evening rush hours (from 7:00 to 9:00 and from 16:30 to 18:30, Local Time) on weekdays (i.e., from Monday to Friday). It required that vehicles with specific tail numbers of the license plates were prohibited on the arterial and residential roads. For instance, the prohibited tail numbers were 1 and 9 on Monday. Other detailed rules were illustrated in Table 1. Second, similar to but more stringent than the routine scenario (S1), the scenario (S2) adopted the even-odd rule to reduce the traffic fluxes in half at the same space. Third, the truck scenario (S3) oriented at both local registered and non-registered trucks, which were strictly prohibited all day long over the highways. Finally, the G20 scenario (S4) reflected the traffic states during the G20 summit in 2016 over the Xiaoshan District, with much stricter traffic limitations than normal situations (Ji et al., 2018; Wang et al., 2020; Zhang et al., 2020). It can be regarded as the combination of the scenario (S2) and the truck scenario (S3).  
170  
175  
180  
Thus, all vehicles should comply with the even-odd rule over the entire district.



## 2.4. Monte Carlo subsampling

The hyperfine bottom-up model was a big-data-driven framework. We should thus apply a sub-  
sampling analysis to evaluate the stability of the resulting on-road vehicle emission inventory. The  
185 objective was to investigate the extent to which less repeated traffic monitoring information can reproduce  
the long-term spatial emission patterns driven by the entire dataset (Apte et al., 2017; Hankey and  
Marshall, 2015).

Here we focus only on weekdays rather than weekends when the expected casual trips might affect  
the analysis. We utilized Monte Carlo simulations to subsample the full-traffic-monitoring-driven  
190 emissions repeatedly. Briefly, we randomly sampled the emission information in unique weekdays ( $1 \leq$   
 $N \leq 42$ ) at each road segment from our universal dataset. Each road segment has 35 weekdays of  
sampling on average. For each value of  $N$ , we performed 1000 random draws to generate 10000  
subsampling “maps” of fine-scale hourly average emissions. For road segments with fewer than  $N$  days of  
sampling, the “subsampling” effectively contained all data. Consequently, the subsampled maps  
195 converged to the full-data-driven results, since  $N$  approached the total number of full traffic monitoring  
information.

We adopted three metrics to compare the performance of each subsampled emission map to that  
of the full-data-driven result. First, as a metric of precision, we calculated the  $\gamma^2$  for them. The second  
metric was the normalized root-mean-square error (i.e., the coefficient of variation of the RMSE,  
200 CVRMSE). Third, as a metric of the temporal stability of sub-sampled spatial patterns, we calculated the  
intraclass correlation (ICC) of each sub-sampled iteration, grouped by road segments. The ICC is a metric  
that results from one-way Analysis of Variance (ANOVA) to quantify the degree of similarity among  
repeated measurements within individual groups (i.e., road segments). After computing the ANOVA for  
data grouped by road segments, the ICC is calculated as the ratio of the variability between groups (Mean  
205 Squares of Treatment/Group, MST) to the sum of the MST and the variability within individual groups  
(Mean Square Error, MSE):

$$ICC = \frac{MST}{MST + MSE} \text{ (Eq. 2).}$$





By definition, ICC is bounded from 0 to 1. For a hypothetical dataset where all repeated measurements at each location were precisely equal to each other, the ICC would converge to 1.0. In contrast, for a dataset  
210 where the concentration variability among repeated measures at each individual location is very high relative to the spatial differences in concentration among roads, the ICC would approach 0. For this application, ICC values of 0.75 ~ 1 reflected large and systematic spatial differences, with low residual temporal variability at each location.

### 3 Results and discussion

#### 215 3.1 Traffic characteristics and hotspots

Comprehensive traffic monitoring, coupled with the ITS, painted vivid pictures of within-urban traffic states, including traffic fluxes, fleet compositions, and traffic speeds (Figs. 3, 4 and Figs. S2 ~ S5). Remarkable spatiotemporal heterogeneities in fine-scale patterns were revealed. First, most (i.e., > 96.49%) of the traffic fluxes concentrated over the arterial roads and the residential streets rather than the  
220 highways (Fig. 3a). Figure 3b illustrates fine-scale variabilities in the traffic fluxes for an indicative ~ 1 km<sup>2</sup> urban zones. Within this small area, the hourly average traffic fluxes varied by more than 15 times. Even within individual roads, they still varied by more than eight times overall. An expected feature throughout the traffic monitoring dataset was the ubiquity of sharp spatial “traffic hotspots” (length < 100 m). Such hotspots were tentatively classified as individual road segments or clusters, where traffic fluxes  
225 exceeded the median level over the whole district. Figure 4 confirms potential causes for an indicative set of hotspots via imagery analysis. A uniform explanation was traffic congestion that, however, resulted from different drivers, such as large traffic fluxes in major arterial roads and their intersections or constructions in the middle of the roads. Such supplemental information provides further details on the hotspot identification scheme.

230 Second, the hourly average traffic fluxes on weekdays were close to those on weekends (Fig. 3 and Fig. S3). Nevertheless, the variation tendencies displayed a distinct picture during different moments between weekdays and weekends (Fig. S2). On weekdays, the diurnal traffic fluxes showed dramatic fluctuations, two peaks at 07:00 and 17:00, obviously related to the morning and evening rush hours. We



noted that such temporal peaks enhanced extensive spatial hotspots, spatially consistent with the above  
235 hotspots based on the hourly average data but quantitatively more prominent (Fig. 3). This was because  
that the morning and evening rush hours deteriorated the traffic congestion (Fig. 4). By comparison, the  
variation extent on weekends was slightly lower than on weekdays and the early peak appeared two hours  
later (Fig. S2). Overall, the maximum peak on weekends barely hit roughly 96.46% of those on weekdays.  
Spatially, the hotspots of the traffic fluxes on weekdays were mostly consistent with those on weekends  
240 but more variable, reflecting frequent casual travels (Fig. S3). Collectively, the fine-scale spatiotemporal  
patterns of traffic fluxes over the entire district, particularly the hotspots, relied more on those on  
weekdays.

Third, significantly strong correlations were found between the traffic speeds and fluxes spatially  
and temporally. Following the traffic fluxes, the simultaneous vehicle-specific speeds fluctuated  
245 substantially throughout the day (Fig. S2). When the traffic fluxes peaked at the morning and evening  
rushes, the vehicle-specific speeds were expected to be at their lowest. Although the peaks changed from  
weekdays to weekends, the valleys kept following such peaks. Spatially, the traffic flux hotspots likely  
determined the traffic speed hotspots, particularly at the morning and evening rush hours (Fig. S4). In  
contrast, the vehicle categories were independent of the traffic fluxes. Their diurnal variations showed  
250 relative stability, even for different road types, after the morning rush hours (Fig. S2 and Fig. 3). On the  
other hand, the HDVs and HDTs peaked in the early hours of the morning (i.e., from 1:00 to 5:00). Besides,  
a striking picture lay in the spatial distributions (Fig. 3 and Fig. S5). The four types of vehicles, including  
LDVs, MDVs, LDTs, and MDTs, flocked over (98.52%) the arterial and residential roads, while the rest  
of vehicle categories, i.e., HDVs and HDTs, concentrated over (3.61%) the highways. Figure 3 details  
255 fine-scale spatial distributions of HDVs and HDTs for three indicative highway zones ( $\sim 1 \text{ km}^2$ ). Therein  
the spatial hotspots scattered extensively. According to the image analysis (Fig. 4), the traffic congestion  
attributed to the large traffic fluxes of HDVs and HDTs should be the unique driver. Therefore, the fleet  
compositions would also affect emission distributions significantly, particularly over fine-scale zones.



### 3.2 Characteristics of on-road vehicle emissions

260 We established a hyperfine-resolution on-road vehicle emission inventory and captured the  
emission hotspots (Fig. 5 and Fig. S6). Overall, the hourly average emissions were summed up based on  
the classified roads (Table S1). It was clear that the emission intensities in the arterial roads, residential  
streets, and highways followed a descending order, although the residential streets were of the longest  
length and the largest traffic fluxes. The leading cause was the difference in vehicle categories in different  
265 road types (Table S1). For instance, we estimated that the hourly average NO<sub>x</sub> emission intensities in the  
arterial roads, residential streets, and highways were 157.76 g/km, 135.22 g/km, and 107.83 g/km,  
respectively. For the highways, the hourly average traffic fluxes were 10277, accounting for 1.99% of the  
total amount, while their emissions amounted to more than 2.04 % of the total emissions.

From the temporal perspective, on-road vehicle emissions of CO, HC, NO<sub>x</sub>, and PM<sub>2.5</sub> showed  
270 similar trends all day (Fig. S7). For instance, the daytime NO<sub>x</sub> emissions accounted for approximately  
85.90% of the daily total emissions. Moreover, the NO<sub>x</sub> emissions varied throughout the day but reached  
agreement among the different road types (i.e., the arterial roads, residential streets, and highways). Yet,  
there was an apparent difference between emissions on weekdays and those on weekends. Similar to the  
temporal variations in the traffic fluxes on weekdays, those in on-road vehicle emissions also peaked at  
275 the morning and evening rush hours. In turn, such temporal patterns were indistinct on weekends.

Spatially, the high hourly average emissions with the unprecedented hyperfine resolution spread all over  
the district (Fig. 5 and Fig. S6). Such spatial pattern was distinct from previous results that generally show  
radiating decreases from the centre to the periphery (Jing et al., 2016; Yang et al., 2019), mostly associated  
with the spatial patterns of the traffic fluxes and vehicle categories (Fig. 3 and Fig. S4). Specifically, the  
280 high emissions at the centre were mainly attributed to the high traffic fluxes and low traffic speeds. Note  
that, on the border of the district, the emission intensities in the residential streets far exceeded (> 436%)  
those in the neighbouring highways. This divergence could be interpreted by the spatial emission  
distributions of different vehicle categories (Fig. 3 and Fig. S5). For instance, the emissions of HDVs and  
HDTs in the residential streets contributed the most (79.79%), much higher than those (1.34%) in the  
285 neighbouring highways.



### 3.4 Emission hotspots and drivers

The emissions of each pollutant (i.e., CO, HC, NO<sub>x</sub>, and PM<sub>2.5</sub>) generally peaked at the major road intersections, leading to the spatial emission hotspots (Fig. 5 and Fig. S6). The highest hourly average emissions occurred at the intersection of two arterial roads (i.e., North Shixin Road and Shanyin Road), where the measurement monitored the largest traffic fluxes (Fig. 3). At broader spatial scales, these hotspot emissions varied substantially among different road types. For instance, the hourly average emissions for the hotspots in Tonghui North Road and Hongda Road (i.e., arterial roads) were approximately consistent with those in Benjing Road and Hongni Road (i.e., residential streets) (Fig. 5 and Fig. S6, arterial roads vs. residential streets: 374.91g/km vs. 216.12g/km CO; 48.90g/km vs. 34.13g/km HC; 180.61g/km vs. 348.38g/km NO<sub>x</sub>; 7.41 vs. 15.81g/km PM<sub>2.5</sub>). In contrast, the hotspot emissions in the arterial roads and highways were substantially elevated above the residential levels. For CO, the hotspot emissions in the highways [arterial roads] exceed those on the residential roads by a factor of 2.1 [2.3]; for HC by a factor of 1.4 [2.6]; for NO<sub>x</sub> by a factor of 0.9 [1.1]; and for PM<sub>2.5</sub> by a factor of 0.8 [1]. Therein, emission hotspots for a given highway road were typically intensive and evident in several areas of the Xiaoshan District (Fig. 5). For instance, we estimated consistently higher (1.2 ~ 2 times) emission levels on a highway (i.e., Airport Road) than those on the neighbouring residential street (i.e., Wenming Road) (Fig. S8). More importantly, the diurnal emission hotspots remained stable spatially (Fig. S9), consistent with the hourly average level (Fig. 5 and Fig. S6). However, the emission intensities of the hotspots varied during different moments between weekdays and weekends (Fig. S10). The higher emissions of hotspots typically appeared at 08:00 and 18:00 on weekdays, 2.2 ~ 3.4 times larger than the hourly average level.

The indicative hotspots over the urban zones generally stretched for 100 ~ 200 m (Fig. 5). Over the short length of the transects, the hourly average emissions rose and fell more than 2.2 times. From the hotspot cores outwards, the hourly average emissions consistently followed “distance-decay” relationships (Fig. 6). An unconstrained three-parameter exponential model,  $E(d) = \alpha + \beta \exp(-3d/k)$ , reproduced the emission-distance relationship  $E(d)$  with high fidelity ( $r^2 = 0.96$ ). Specifically, the isotropic parameter  $d$  reflected the distance to the hotspot cores ( $m$ ); the background parameter  $\alpha$  represented the background emissions far from the hotspots ( $d \rightarrow 1000m$ ); the parameter  $\beta$  represented



the emission increment resulting from proximity to the hotspots; the decay parameter  $k$  governed the  
315 spatial scale over which emissions relaxed to  $\alpha$ . For all pollutants, estimated values of  $(\alpha + \beta)$   
approached a constant (1.0), indicating that the combined contribution of the background and the near-  
hotspot increment approached the hotspot emission levels.

Figure 6 shows the decay patterns of the hourly average emissions over urban zones on weekdays.  
These results reflected the hourly average emission ratios (normalized at the hourly average emissions of  
320 the hotspots) from hotspots outwards as a function of the distance ( $d$ ). Note that the ratios of the hourly  
average traffic fluxes and vehicle category proportions were calculated in the same way.

Consistent with expectations about the speed-dependent emission factors (Fig. S1), our estimated  
distance-decay relationships were sharpest for  $\text{NO}_x$ , intermediate for HC and  $\text{PM}_{2.5}$ , and most shallow for  
CO. In theory, comprehensive traffic profiles underlay the estimated hotspot emissions. To elucidate  
325 determinants of the emission hotspot patterns, we mined those traffic data (Fig. 3, Fig. 5, and Fig. S6).  
As expected, we found that the traffic fluxes largely shaped the spatial emission hotspot patterns over the  
arterial and residential roads. Besides, the specific vehicle categories (i.e., HDVs and HDTs) also play a  
key role.

For the emission hotspots in the highways, the traffic fluxes and emissions were both distance-  
330 dependent and applicable to the “distance-decay” exponential models, while the vehicle categories were  
consistently stable (Fig. 6). This demonstrates that the traffic fluxes played a cardinal role in determining  
the spatial emission hotspot patterns over the highways. In contrast, in the arterial and residential roads,  
coincident peaks of the specific vehicle categories (i.e., HDVs and HDTs) and traffic fluxes corresponded  
in space to the emission hotspots (Fig. 6). This reveals that, besides the traffic fluxes, the specific vehicle  
335 categories (i.e., HDVs and HDTs) also substantially contributed to the high emissions over the arterial  
and residential roads.

### 3.5 Impacts of traffic control scenarios

Four scenarios (i.e., S1 ~ S4) demonstrated substantial impacts of traffic management on  
340 spatiotemporal traffic states (Fig. S11). Therein the S1 and S2 scenarios focused on reducing the traffic



fluxes, while the S3 and S4 scenarios gave full consideration to not only the traffic fluxes but also the fleet compositions (Table 1). Without strict traffic restrictions, the S1 scenario only reduced the traffic fluxes by 3.82 % and showed no significant effects on the traffic flux hotspots. On this basis, the traffic fluxes were further decreased by 9.56 % under the S2 scenario. Most of the traffic flux hotspots vanished.  
345 Under the S3 scenario, the fleet compositions were changed evidently over the highways, where HDTs and HDVs were removed. The S4 scenario combined the exclusive settings in the S2 and S3 scenarios and thus realized their consequences. This scenario achieved further decreases in the traffic fluxes (51.3%).

This study estimated that the daily average on-road vehicle emissions were 3.40 tons for CO, 0.482 tons for HC, 2.306 tons for NO<sub>x</sub>, and 0.097 tons for PM<sub>2.5</sub> (Fig. 7 and Fig. S12). Under the S1  
350 scenario, the daily average emissions decreased by small percentages (i.e., 3.74% for CO, 3.43% for HC, 3.13% for NO<sub>x</sub>, and 3.08% for PM<sub>2.5</sub>). Compared with the S1 scenario, the S2 scenario led to significant reductions over the arterial and residential roads (i.e., 9.34% for CO, 8.59% for HC, 7.83% for NO<sub>x</sub>, and 7.69% for PM<sub>2.5</sub>). This represents the effects of strictly traffic flux controls on on-road  
355 vehicle emissions, particularly over the urban zones. The S3 scenario reveals that the HDVs and HDTs were responsible for a major part (15.94 ~ 57.50%) of CO, NO<sub>x</sub>, PM<sub>2.5</sub>, and HC emissions over the highways. On this basis, the S4 scenario adopted comprehensive traffic controls, thus reducing roughly additional emissions (i.e., 50.77% for CO, 67.44% for HC, 82.72% for NO<sub>x</sub>, and 84.20% for PM<sub>2.5</sub>). As a result, the emission hotspots over all roads were mostly removed.

### 360 **3.6 Comparison with other inventories**

The bottom-up on-road vehicle emissions in this study were compared with conventional emission inventories (i.e., MEICv1.3 for 2016 and HTAPv2.2 for 2010) (Fig. S13) (Janssens-Maenhout et al., 2015; Li et al., 2017). It should be noted that the spatial resolution of MEICv1.3 and HTAPv2.2 was roughly 0.25° \* 0.25° and 0.1° \* 0.1°, respectively. Hence, the total emissions over the Xiaoshan District were re-  
365 aggregated with area-weighting. It was clear that the monthly average on-road vehicle emissions in this study were significantly lower than those in MEICv1.3 and HTAPv2.2 (i.e., MEIC: 14.8% for CO, 30.1% for HC, 40.1% for NO<sub>x</sub>, and 19.7% for PM<sub>2.5</sub>. HTAP: 22.4% for CO, 44.5% for HC, 67.7% for NO<sub>x</sub> and



29.1% for PM<sub>2.5</sub>). This could be attributed to the on-road vehicle emission mitigation measures in China. Moreover, owing to the limitation of the spatial resolution, these conventional inventories were incapable of depicting the emission hotspots over the Xiaoshan District. Such limitations could be propagated to previous CTM simulations driven by those conventional inventories, thus unable to reproduce the fine-scale on-road vehicle emissions.

### 3.7 Stability Analysis

Through systematic subsampling of our weekday emission dataset, we found that 15 ~ 30 weekdays were sufficient to reproduce key spatial patterns with good precision and low bias (Figure 8). The following trends hold: a small number of drive days ( $N < 5$ ) typically resulted in a poor approximation of long-term spatial patterns from the full data set, with generally low precision ( $\gamma^2$ ) and high bias (CV-RMSE). However, each additional sampling day resulted in a substantial improvement in  $\gamma^2$  and CV-RMSE.

For our dataset, diminishing returns for improvement in  $\gamma^2$  set in at 15 ~ 25 drive days, with mean  $\gamma^2$  for NO<sub>x</sub> and PM<sub>2.5</sub> approaching 0.7 after 15 weekdays, and approaching 0.9 after 30 ~ 35 weekdays. We found that ICC values ranged from 0.72 to 0.91 for all pollutants (Table S2). This indicates that our measurement-based long-term spatial patterns were robust to stochastic variability among those samples. Average values of ICC (Figure S14) were generally high for 10 or fewer weekdays, indicating that stochastic temporal variability from a small number of weekdays did not obscure an overall spatially dominated emission pattern. Note that our sampling was restricted to weekday conditions, while spatial patterns may differ at other times (weekends) due to casual trips. Future work may reveal whether similar scaling considerations hold over a broader range of conditions.

## 4 Conclusions

In this study, comprehensive traffic conditions are fully measured and interconnected via the ITS. We find the spatial variabilities existing at much finer scales (i.e., 10m ~ 1km). Further, we capture the emission hotspots generally driven by high traffic fluxes. Over the highways, they are also associated with the distributions of HDVs and HDTs. Such findings might be missed by conventionally sparse



sampling and previous model predictions. Overall, routine accessibility of hyperfine-resolution on-road  
395 vehicle emissions could have transformative implications for air pollution control, urban management  
and policymaking, epidemiology, and public awareness (Daellenbach et al., 2020; Dedoussi et al., 2020;  
Geng et al., 2019; Nyhan et al., 2016; Yang and Zhang, 2018; Zeger et al., 2000). By pinpointing localized  
emission hotspots, these data may provide new opportunities for air pollution control. In turn, Street-level  
emission data can complement, challenge, and validate other emission and air quality datasets, including  
400 CTM outputs and near-road air quality measurements (Apte et al., 2017; Grange et al., 2017; Jiang et al.,  
2018; Yang et al., 2018a). Moreover, such refinements can help address exposure misclassification and  
even directly alter personal behaviour, much as real-time traffic navigation data now inform individual  
driving patterns. In addition, this hyperfine-resolution on-road vehicle emissions and subsequent air  
quality maps might result in broader societal consequences, including urban land-use decisions,  
405 ecological planning, and political economy.





**Data availability.** Traffic monitoring data and model results are available upon request.

**Supplement.** The supplement related to this article is available online.

410

**Author contributions.** S. Y., P. L. conceived and designed the research. L. J. performed model simulations. Y. X., X. C., L. W., and J. Y. conducted data analysis. T. H., L. W., Y. Z., M. L., Z. L., Z. S., Y. J., W. L., D. R., and J. H. S contributed to the scientific discussions. S. Y., P. L., and J. H. S wrote and revised the manuscript.

415 **Competing interests.** The authors declare that they have no conflict of interest.

**Acknowledgements.** This study is supported by the Department of Science and Technology of China (No. 2016YFC0202702, 2018YFC0213506 and 2018YFC0213503), National Research Program for Key Issues in Air Pollution Control in China (No. DQGG0107) and National Natural Science Foundation of China (No. 21577126 and 41561144004). Pengfei Li is supported  
420 by Initiation Fund for Introducing Talents of Hebei Agricultural University (412201904), Hebei Youth Top Fund (BJ2020032), and National Natural Science Foundation of China (No. 22006030).

## References

- Anenberg, S. C., Miller, J., Minjares, R., Du, L., Henze, D. K., Lacey, F., Malley, C. S., Emberson, L., Franco, V., Klimont, Z. and Heyes, C.: Impacts and mitigation of excess diesel-related NO<sub>x</sub> emissions in 11 major vehicle markets, *Nature*,  
425 545(7655), 467–471, doi:10.1038/nature22086, 2017.
- Apte, J. S., Messier, K. P., Gani, S., Brauer, M., Kirchstetter, T. W., Lunden, M. M., Marshall, J. D., Portier, C. J., Vermeulen, R. C. H. and Hamburg, S. P.: High-Resolution Air Pollution Mapping with Google Street View Cars: Exploiting Big Data, *Environ. Sci. Technol.*, 51(12), 6999–7008, doi:10.1021/acs.est.7b00891, 2017.
- Avila, A. M. and Mezić, I.: Data-driven analysis and forecasting of highway traffic dynamics, *Nat. Commun.*, 11(1), 2090,  
430 doi:10.1038/s41467-020-15582-5, 2020.
- Chen, J., Li, W., Zhang, H., Jiang, W., Li, W., Sui, Y., Song, X. and Shibasaki, R.: Mining urban sustainable performance: GPS data-based spatio-temporal analysis on on-road braking emission, *J. Clean. Prod.*, 270, 122489, doi:https://doi.org/10.1016/j.jclepro.2020.122489, 2020.
- Daellenbach, K. R., Uzu, G., Jiang, J., Cassagnes, L.-E., Leni, Z., Vlachou, A., Stefanelli, G., Canonaco, F., Weber, S.,  
435 Segers, A., Kuenen, J. J. P., Schaap, M., Favez, O., Albinet, A., Aksoyoglu, S., Dommen, J., Baltensperger, U., Geiser, M., El Haddad, I., Jaffrezo, J.-L. and Prévôt, A. S. H.: Sources of particulate-matter air pollution and its oxidative potential in Europe, *Nature*, 587(7834), 414–419, doi:10.1038/s41586-020-2902-8, 2020.



- Dedoussi, I. C., Eastham, S. D., Monier, E. and Barrett, S. R. H.: Premature mortality related to United States cross-state air pollution, *Nature*, 578(7794), 261–265, doi:10.1038/s41586-020-1983-8, 2020.
- 440 Deng, F., Lv, Z., Qi, L., Wang, X., Shi, M. and Liu, H.: A big data approach to improving the vehicle emission inventory in China, *Nat. Commun.*, 11(1), 2801, doi:10.1038/s41467-020-16579-w, 2020.
- Gately, C. K. and Hutyra, L. R.: Large Uncertainties in Urban-Scale Carbon Emissions, *J. Geophys. Res. Atmos.*, 122(20), 11,211–242,260, doi:https://doi.org/10.1002/2017JD027359, 2017.
- Gately, C. K., Hutyra, L. R., Wing, I. S. and Brondfield, M. N.: A Bottom up Approach to on-Road CO<sub>2</sub> Emissions  
445 Estimates: Improved Spatial Accuracy and Applications for Regional Planning, *Environ. Sci. Technol.*, 47(5), 2423–2430, doi:10.1021/es304238v, 2013.
- Gately, C. K., Hutyra, L. R., Peterson, S. and Sue Wing, I.: Urban emissions hotspots: Quantifying vehicle congestion and air pollution using mobile phone GPS data, *Environ. Pollut.*, 229, 496–504, doi:https://doi.org/10.1016/j.envpol.2017.05.091, 2017.
- 450 Geng, G., Xiao, Q., Zheng, Y., Tong, D., Zhang, Y., Zhang, X., Zhang, Q., He, K. and Liu, Y.: Impact of China’s Air Pollution Prevention and Control Action Plan on PM<sub>2.5</sub> chemical composition over eastern China, *Sci. China Earth Sci.*, 62(12), 1872–1884, doi:10.1007/s11430-018-9353-x, 2019.
- Grange, S. K., Lewis, A. C., Moller, S. J. and Carslaw, D. C.: Lower vehicular primary emissions of NO<sub>2</sub> in Europe than assumed in policy projections, *Nat. Geosci.*, 10(12), 914–918, doi:10.1038/s41561-017-0009-0, 2017.
- 455 Hankey, S. and Marshall, J. D.: Land Use Regression Models of On-Road Particulate Air Pollution (Particle Number, Black Carbon, PM<sub>2.5</sub>, Particle Size) Using Mobile Monitoring, *Environ. Sci. Technol.*, 49(15), 9194–9202, doi:10.1021/acs.est.5b01209, 2015.
- He, G., Pan, Y. and Tanaka, T.: The short-term impacts of COVID-19 lockdown on urban air pollution in China, *Nat. Sustain.*, 3(12), 1005–1011, doi:10.1038/s41893-020-0581-y, 2020.
- 460 Hua, X.-S.: The City Brain: Towards Real-Time Search for the Real-World, in *The 41st International ACM SIGIR Conference on Research & Development in Information Retrieval*, pp. 1343–1344, Association for Computing Machinery, New York, NY, USA., 2018.
- Huang, Y., Surawski, N. C., Yam, Y.-S., Lee, C. K. C., Zhou, J. L., Organ, B. and Chan, E. F. C.: Re-evaluating effectiveness of vehicle emission control programmes targeting high-emitters, *Nat. Sustain.*, 3(11), 904–907,  
465 doi:10.1038/s41893-020-0573-y, 2020.
- International Council on Clean Transportation (ICCT): China’s vehicle emissions inspection and maintenance program., 2020.
- Janssens-Maenhout, G., Crippa, M., Guizzardi, D., Dentener, F., Muntean, M., Pouliot, G., Keating, T., Zhang, Q., Kurokawa, J., Wankmüller, R. and others: HTAP\_v2. 2: a mosaic of regional and global emission grid maps for 2008 and  
470 2010 to study hemispheric transport of air pollution, *Atmos. Chem. Phys.*, 15(19), 11411–11432, 2015.



- Ji, Y., Qin, X., Wang, B., Xu, J., Shen, J., Chen, J., Huang, K., Deng, C., Yan, R., Xu, K. and others: Counteractive effects of regional transport and emission control on the formation of fine particles: a case study during the Hangzhou G20 summit, *Atmos. Chem. Phys.*, 18(18), 13581–13600, 2018.
- Jiang, Z., McDonald, B. C., Worden, H., Worden, J. R., Miyazaki, K., Qu, Z., Henze, D. K., Jones, D. B. A., Arellano, A. F.,  
475 Fischer, E. V and others: Unexpected slowdown of US pollutant emission reduction in the past decade, *Proc. Natl. Acad. Sci.*, 115(20), 5099–5104, 2018.
- Jing, B., Wu, L., Mao, H., Gong, S., He, J., Zou, C., Song, G., Li, X. and Wu, Z.: Development of a vehicle emission inventory with high temporal–spatial resolution based on NRT traffic data and its impact on air pollution in Beijing – Part 1: Development and evaluation of vehicle emission inventory, *Atmos. Chem. Phys.*, 16(5), 3161–3170, doi:10.5194/acp-16-  
480 3161-2016, 2016.
- Kelly, F. J. and Zhu, T.: Transport solutions for cleaner air, *Science* (80-. ), 352(6288), 934 LP – 936, doi:10.1126/science.aaf3420, 2016.
- Lelieveld, J., Evans, J. S., Fnais, M., Giannadaki, D. and Pozzer, A.: The contribution of outdoor air pollution sources to premature mortality on a global scale, *Nature*, 525(7569), 367–371, doi:10.1038/nature15371, 2015.
- 485 Li, M., Zhang, Q., Kurokawa, J., Woo, J.-H., He, K., Lu, Z., Ohara, T., Song, Y., Streets, D. G., Carmichael, G. R. and others: MIX: a mosaic Asian anthropogenic emission inventory under the international collaboration framework of the MICS-Asia and HTAP, *Atmos. Chem. Phys.*, 17(2), 2017.
- Liu, J., Han, K., Chen, X. (Michael) and Ong, G. P.: Spatial-temporal inference of urban traffic emissions based on taxi trajectories and multi-source urban data, *Transp. Res. Part C Emerg. Technol.*, 106, 145–165,  
490 doi:<https://doi.org/10.1016/j.trc.2019.07.005>, 2019.
- Liu, Y.-H., Ma, J.-L., Li, L., Lin, X.-F., Xu, W.-J. and Ding, H.: A high temporal-spatial vehicle emission inventory based on detailed hourly traffic data in a medium-sized city of China, *Environ. Pollut.*, 236, 324–333, doi:<https://doi.org/10.1016/j.envpol.2018.01.068>, 2018.
- Nyhan, M., Grauwlin, S., Britter, R., Misstear, B., McNabola, A., Laden, F., Barrett, S. R. H. and Ratti, C.: “Exposure  
495 Track”—The Impact of Mobile-Device-Based Mobility Patterns on Quantifying Population Exposure to Air Pollution, *Environ. Sci. Technol.*, 50(17), 9671–9681, doi:10.1021/acs.est.6b02385, 2016.
- Paul, J., Malhotra, B., Dale, S. and Qiang, M.: RFID based vehicular networks for smart cities, in 2013 IEEE 29th International Conference on Data Engineering Workshops (ICDEW), pp. 120–127., 2013.
- Song, J., Zhao, C., Lin, T., Li, X. and Prishchepov, A. V: Spatio-temporal patterns of traffic-related air pollutant emissions in  
500 different urban functional zones estimated by real-time video and deep learning technique, *J. Clean. Prod.*, 238, 117881, doi:<https://doi.org/10.1016/j.jclepro.2019.117881>, 2019.
- Tessum, C. W., Hill, J. D. and Marshall, J. D.: Life cycle air quality impacts of conventional and alternative light-duty transportation in the United States, *Proc. Natl. Acad. Sci.*, 111(52), 18490 LP – 18495, doi:10.1073/pnas.1406853111, 2014.



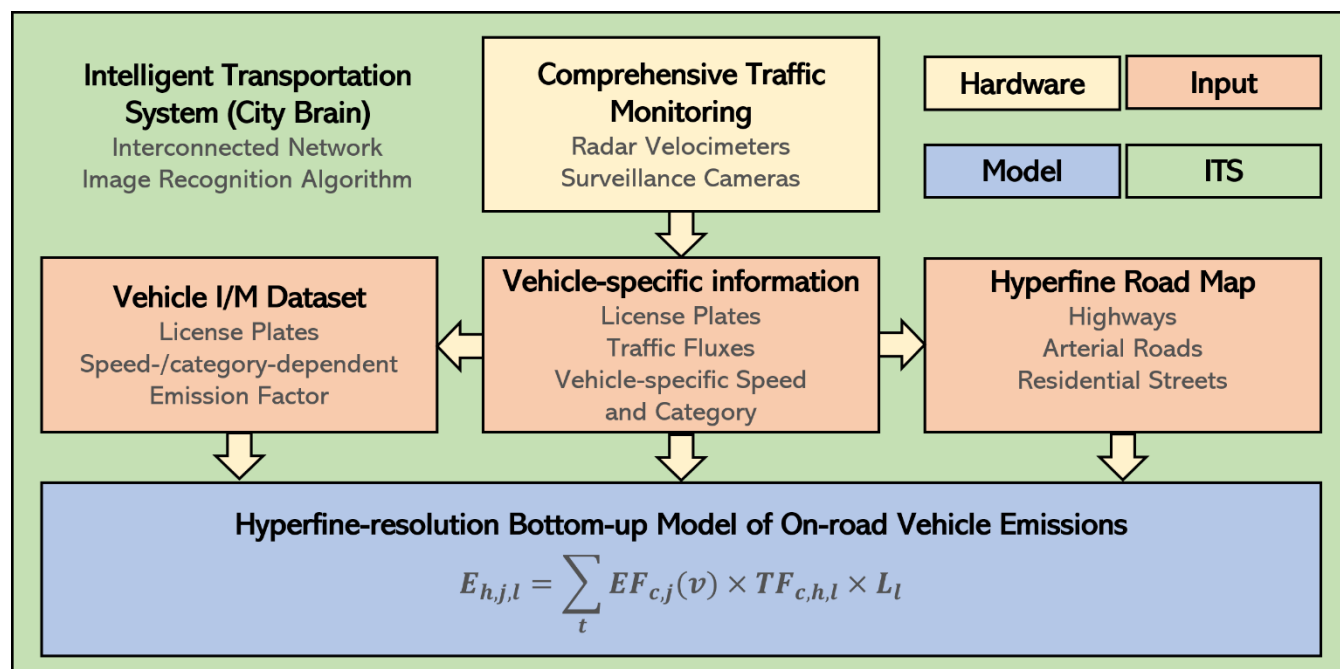
- 505 Wang, L., Yu, S., Li, P., Chen, X., Li, Z., Zhang, Y., Li, M., Mehmood, K., Liu, W., Chai, T., Zhu, Y., Rosenfeld, D. and Seinfeld, J. H.: Significant wintertime PM<sub>2.5</sub> mitigation in the Yangtze River Delta, China from 2016 to 2019: observational constraints on anthropogenic emission controls, *Atmos. Chem. Phys.*, 2020, 1–31, doi:10.5194/acp-2020-510, 2020.
- Wen, Y., Zhang, S., Zhang, J., Bao, S., Wu, X., Yang, D. and Wu, Y.: Mapping dynamic road emissions for a megacity by using open-access traffic congestion index data, *Appl. Energy*, 260, 114357, doi:https://doi.org/10.1016/j.apenergy.2019.114357, 2020.
- 510 West, J. J., Fiore, A. M., Horowitz, L. W. and Mauzerall, D. L.: Global health benefits of mitigating ozone pollution with methane emission controls, *Proc. Natl. Acad. Sci. U. S. A.*, 103(11), 3988 LP – 3993, doi:10.1073/pnas.0600201103, 2006.
- Wu, L., Chang, M., Wang, X., Hang, J. and Zhang, J.: Development of a real-time on-road emission (ROE v1.0) model for street-scale air quality modeling based on dynamic traffic big data, *Geosci. Model Dev. Discuss.*, 1–19, doi:10.5194/gmd-2019-74, 2019.
- 515 Yang, B., Zhang, K. M., Xu, W. D., Zhang, S., Batterman, S., Baldauf, R. W., Deshmukh, P., Snow, R., Wu, Y., Zhang, Q., Li, Z. and Wu, X.: On-Road Chemical Transformation as an Important Mechanism of NO<sub>2</sub> Formation, *Environ. Sci. Technol.*, 52(8), 4574–4582, doi:10.1021/acs.est.7b05648, 2018a.
- Yang, D., Zhang, S., Niu, T., Wang, Y., Xu, H., Zhang, K. M. and Wu, Y.: High-resolution mapping of vehicle emissions of atmospheric pollutants based on large-scale, real-world traffic datasets, *Atmos. Chem. Phys.*, 19(13), 8831–8843, doi:10.5194/acp-19-8831-2019, 2019.
- 520 Yang, J. and Zhang, B.: Air pollution and healthcare expenditure: Implication for the benefit of air pollution control in China, *Environ. Int.*, 120, 443–455, doi:https://doi.org/10.1016/j.envint.2018.08.011, 2018.
- Yang, W., Yu, C., Yuan, W., Wu, X., Zhang, W. and Wang, X.: High-resolution vehicle emission inventory and emission control policy scenario analysis, a case in the Beijing-Tianjin-Hebei (BTH) region, China, *J. Clean. Prod.*, 203, 530–539, doi:https://doi.org/10.1016/j.jclepro.2018.08.256, 2018b.
- 525 Yang, Z., Peng, J., Wu, L., Ma, C., Zou, C., Wei, N., Zhang, Y., Liu, Y., Andre, M., Li, D. and Mao, H.: Speed-guided intelligent transportation system helps achieve low-carbon and green traffic: Evidence from real-world measurements, *J. Clean. Prod.*, 268, 122230, doi:https://doi.org/10.1016/j.jclepro.2020.122230, 2020.
- 530 Yu, Q., Zhang, H., Li, W., Song, X., Yang, D. and Shibasaki, R.: Mobile phone GPS data in urban customized bus: Dynamic line design and emission reduction potentials analysis, *J. Clean. Prod.*, 272, 122471, doi:https://doi.org/10.1016/j.jclepro.2020.122471, 2020.
- Zeger, S. L., Thomas, D., Dominici, F., Samet, J. M., Schwartz, J., Dockery, D. and Cohen, A.: Exposure measurement error in time-series studies of air pollution: concepts and consequences., *Environ. Health Perspect.*, 108(5), 419–426, doi:10.1289/ehp.00108419, 2000.
- 535 Zhang, G., Xu, H., Wang, H., Xue, L., He, J., Xu, W., Qi, B., Du, R., Liu, C., Li, Z., Gui, K., Jiang, W., Liang, L., Yan, Y. and Meng, X.: Exploring the inconsistent variations in atmospheric primary and secondary pollutants during the 2016 G20



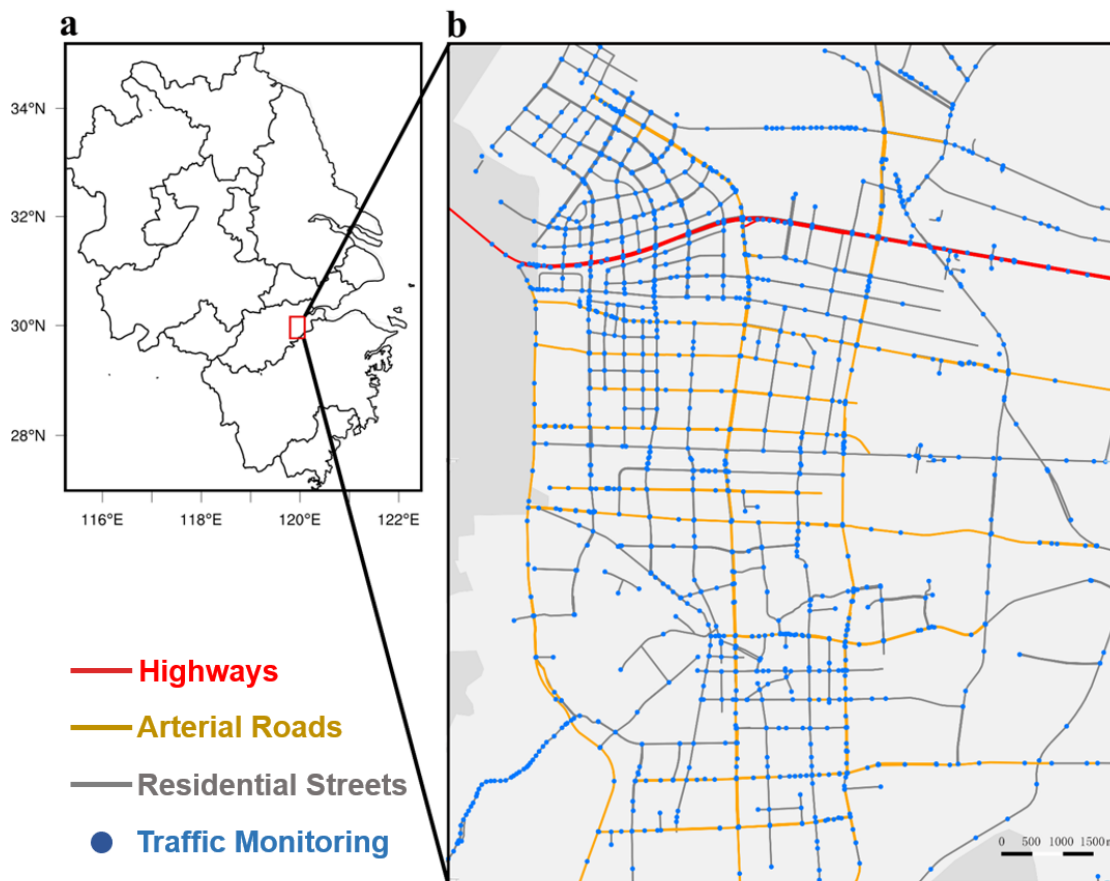
- summit in Hangzhou, China: implications from observations and models, *Atmos. Chem. Phys.*, 20(9), 5391–5403, doi:10.5194/acp-20-5391-2020, 2020.
- Zhang, Q., He, K. and Huo, H.: Policy: cleaning China’s air, *Nature*, 484(7393), 161, 2012.
- 540 Zhang, Q., Zheng, Y., Tong, D., Shao, M., Wang, S., Zhang, Y., Xu, X., Wang, J., He, H., Liu, W., Ding, Y., Lei, Y., Li, J., Wang, Z., Zhang, X., Wang, Y., Cheng, J., Liu, Y., Shi, Q., Yan, L., Geng, G., Hong, C., Li, M., Liu, F., Zheng, B., Cao, J., Ding, A., Gao, J., Fu, Q., Huo, J., Liu, B., Liu, Z., Yang, F., He, K. and Hao, J.: Drivers of improved PM<sub>2.5</sub> air quality in China from 2013 to 2017, *Proc. Natl. Acad. Sci.*, 116(49), 24463 LP – 24469, doi:10.1073/pnas.1907956116, 2019.
- 545 Zhang, S., Wu, Y., Liu, H., Wu, X., Zhou, Y., Yao, Z., Fu, L., He, K. and Hao, J.: Historical evaluation of vehicle emission control in Guangzhou based on a multi-year emission inventory, *Atmos. Environ.*, 76, 32–42, doi:<https://doi.org/10.1016/j.atmosenv.2012.11.047>, 2013.
- Zhang, S., Wu, Y., Huang, R., Wang, J., Yan, H., Zheng, Y. and Hao, J.: High-resolution simulation of link-level vehicle emissions and concentrations for air pollutants in a traffic-populated eastern Asian city, *Atmos. Chem. Phys.*, 16(15), 9965–
- 550 9981, doi:10.5194/acp-16-9965-2016, 2016.
- Zhang, S., Niu, T., Wu, Y., Zhang, K. M., Wallington, T. J., Xie, Q., Wu, X. and Xu, H.: Fine-grained vehicle emission management using intelligent transportation system data, *Environ. Pollut.*, 241, 1027–1037, doi:<https://doi.org/10.1016/j.envpol.2018.06.016>, 2018.



555



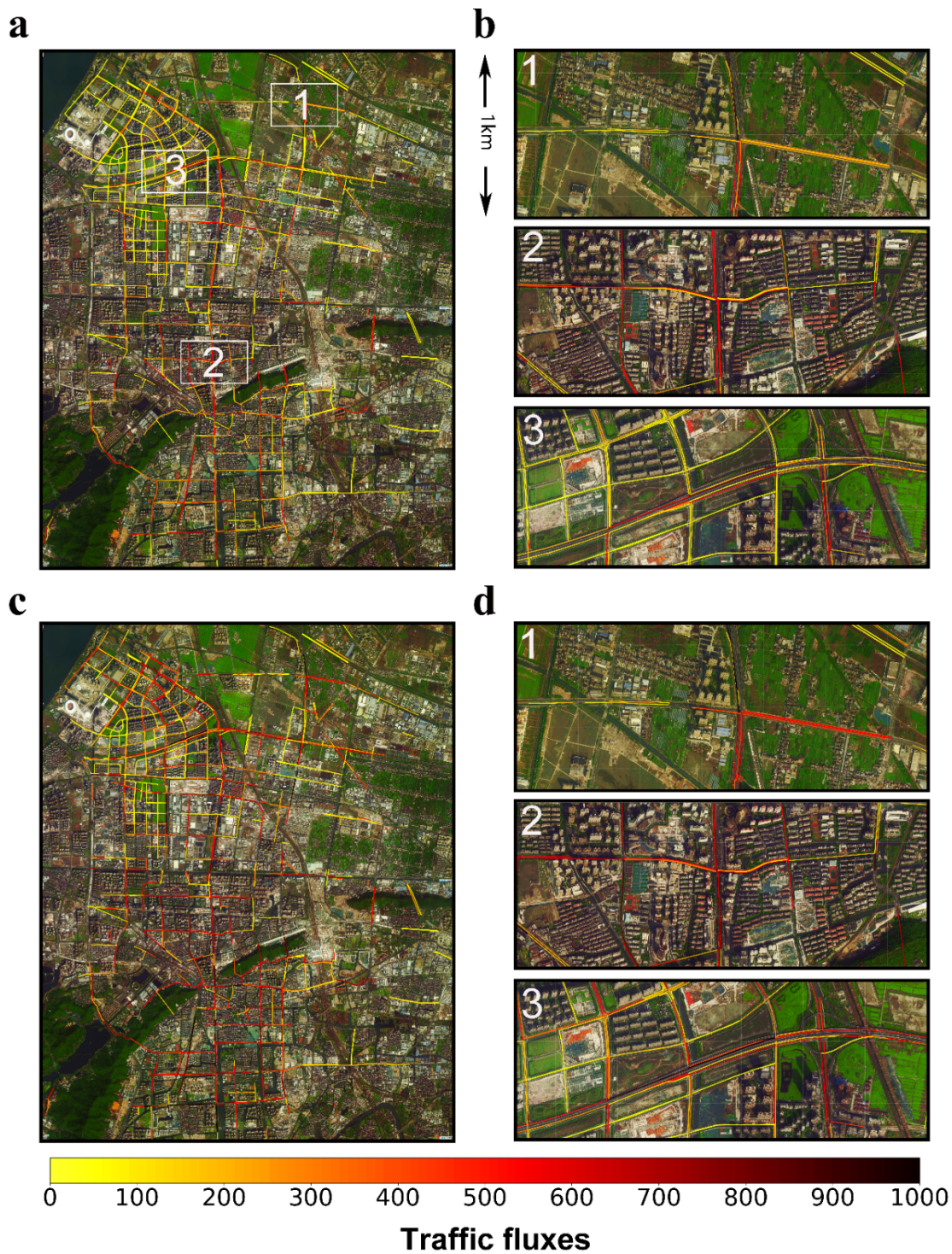
**Figure 1. A hyperfine-resolution bottom-up model framework for on-road vehicle emissions.** Each set of comprehensive traffic monitoring includes radar velocimeters and surveillance cameras. Consequently, vehicle-specific information is collected, including license plates, speed, categories, and traffic fluxes. According to the license plates, the speed-/category-dependent emission factors are obtained from the local official vehicle I/M dataset. Over the entire district, road segments are divided into three road classes: highways, arterial roads, and residential streets. Each road segment is adaptive to a set of traffic monitoring that can collect comprehensive traffic profiles. Therefore, all-round traffic monitoring produces the hyperfine-resolution road map. On the basis of these input data, a hyperfine-resolution bottom-up model framework is established to calculate primary on-road vehicle emissions. The detailed information is illustrated in Sect. 2.2. Here, an intelligent transportation system (ITS) (named “City Brain”) is developed to interconnect these input data. In addition, an image recognition algorithm is embedded to recognize the category for a certain vehicle.



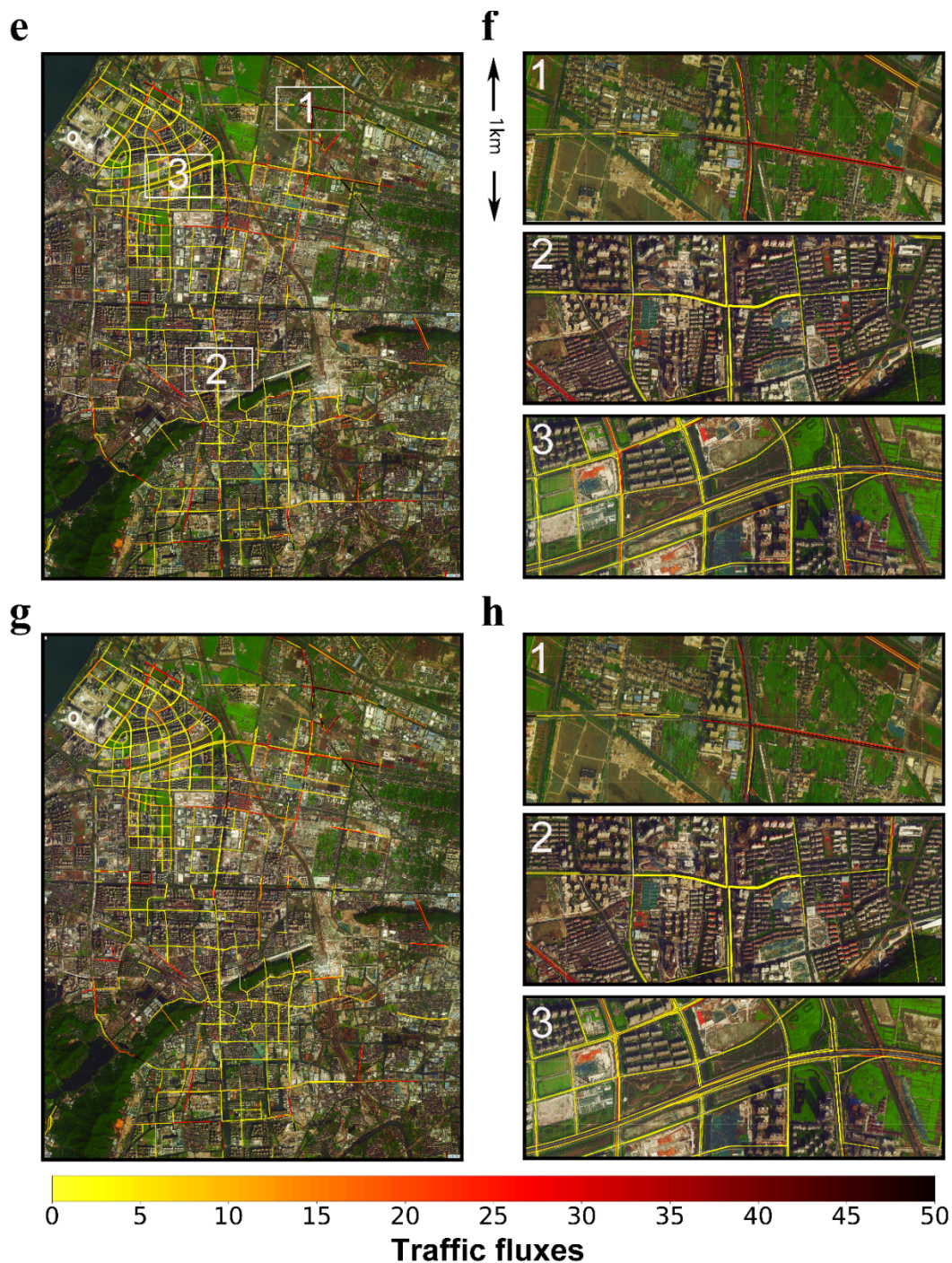
**Figure 2. Comprehensive traffic monitoring network in the Xiaoshan District. (a)** The Xiaoshan District (the red

570 rectangle) is located in the hinterland of the YRD in China. **(b)** Comprehensive traffic monitoring achieves full coverage over the Xiaoshan District. Each dot represents a set of comprehensive traffic monitoring that can recognize traffic fluxes, vehicle-specific speed, categories, and license plates. The gaps between two sets, ranging from 10 m to 1 km, determine the spatial resolution of the road and emission map. The entire road network over the Xiaoshan District is divided into 1894 road segments. Such road segments are divided into three road classes: highways (red lines), arterial

575 roads (yellow lines), and residential streets (grey lines). Map data © 2021, Gaode Map.







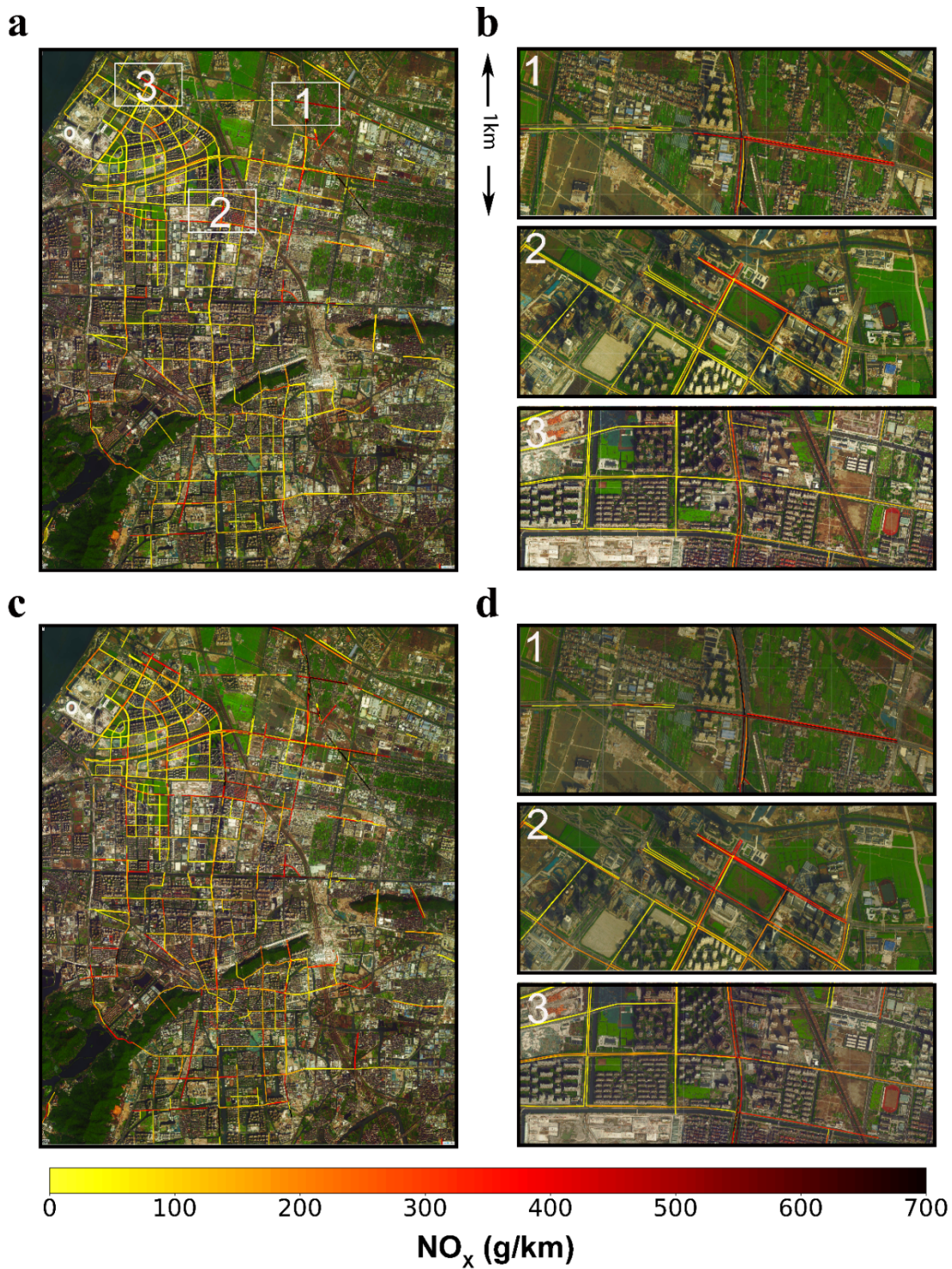
580 **Figure 3. Hyperfine-resolution mapping of observed traffic fluxes.** (a) Hourly average traffic fluxes in each road segment based on two-month traffic monitoring data over the entire district and (b) for three indicative 1 km<sup>2</sup>



585 urban zones therein. The subgraphs (c) and (d) are as the same as (a) and (b) but for the hourly average traffic fluxes during the morning and evening rush hours (from 7:00 to 9:00 and from 16:30 to 18:30, Local Time) on weekdays (from Monday to Friday). The subgraphs (e) and (f) are as the same as (a) and (b) but for the hourly average traffic fluxes of HDVs and HDTs. The subgraphs (g) and (h) are as the same as (c) and (f) but for the morning and evening rush hours on weekdays. The indicative zones are marked by white rectangles in (a) and their spatial scales are presented in (b). Illustrative traffic hotspots (circles) are also annotated in (a), including Tonghui North Road, Hongda Road, Shixin North Road, Shanyin Road, and Airport Road. Map data © 2021, Gaode Map.



590 **Figure 4.** Imagery analysis for illustrative traffic hotspots. (a ~ b) Over the hotspots in the urban zones, frequent large traffic fluxes are identified in major arterial roads and their intersections. (c) Constructions in the middle of the roads also lead to traffic congestion. (d ~ e) Morning and afternoon traffic rushes further deteriorate traffic congestion. (f) Over the highways, the hotspots are related to large traffic fluxes of MDTs and HDTs. The vehicle licence plates are pixelated. The hotspot locations are presented in Fig. 3.



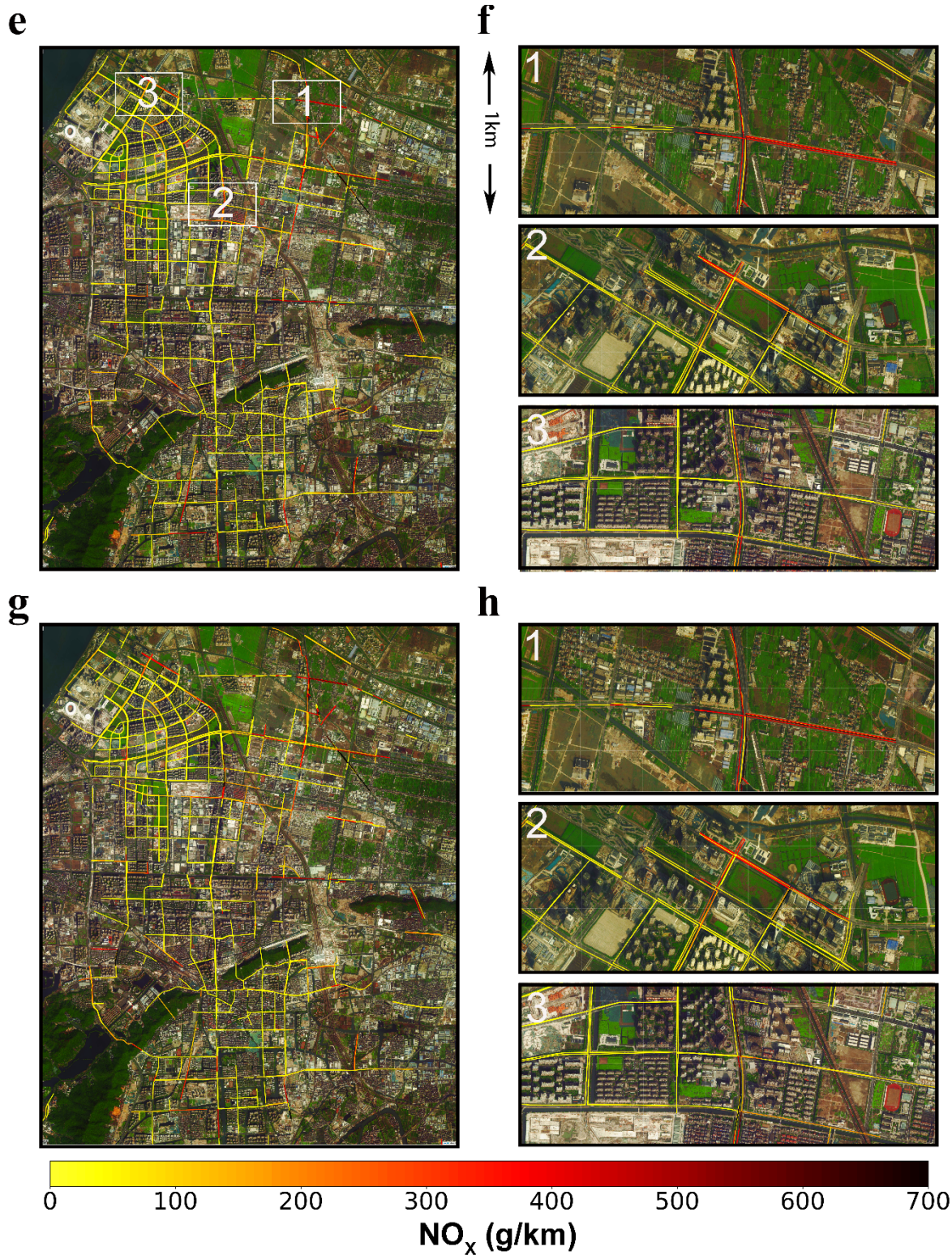
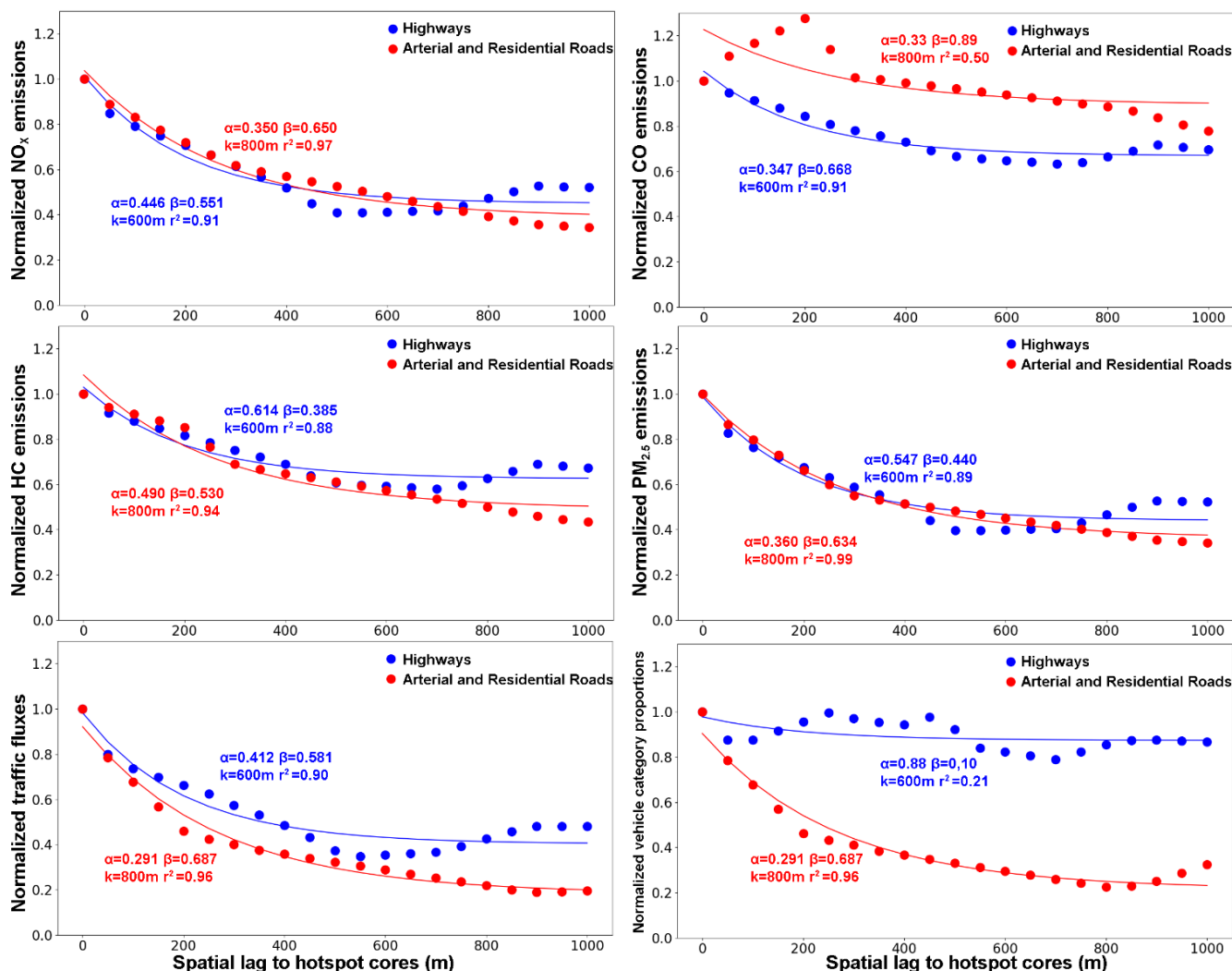




**Figure 5. Hyperfine-resolution mapping of on-road vehicle emissions.** (a) Hourly average on-road vehicle NO<sub>x</sub> emissions for each road segment based on two-month traffic monitoring data for the entire district and (b) for three indicative 2.5 km<sup>2</sup> urban zones therein. The subgraphs (c) and (d) are as the same as (a) and (b) but for the hourly average emissions during the morning and evening rush hours (from 7:00 to 9:00 and from 16:30 to 18:30, Local Time) on weekdays (from Monday to Friday). The subgraphs (e) and (f) are as the same as (a) and (b) but for the hourly average emissions of HDTs and HDVs. The subgraphs (g) and (h) are as the same as (a) and (b) but for the hourly average emissions of HDTs and HDVs during the morning and evening rush hours on weekdays. The indicative zones are marked by white rectangles in (a). Map data © 2021, Gaode Map.

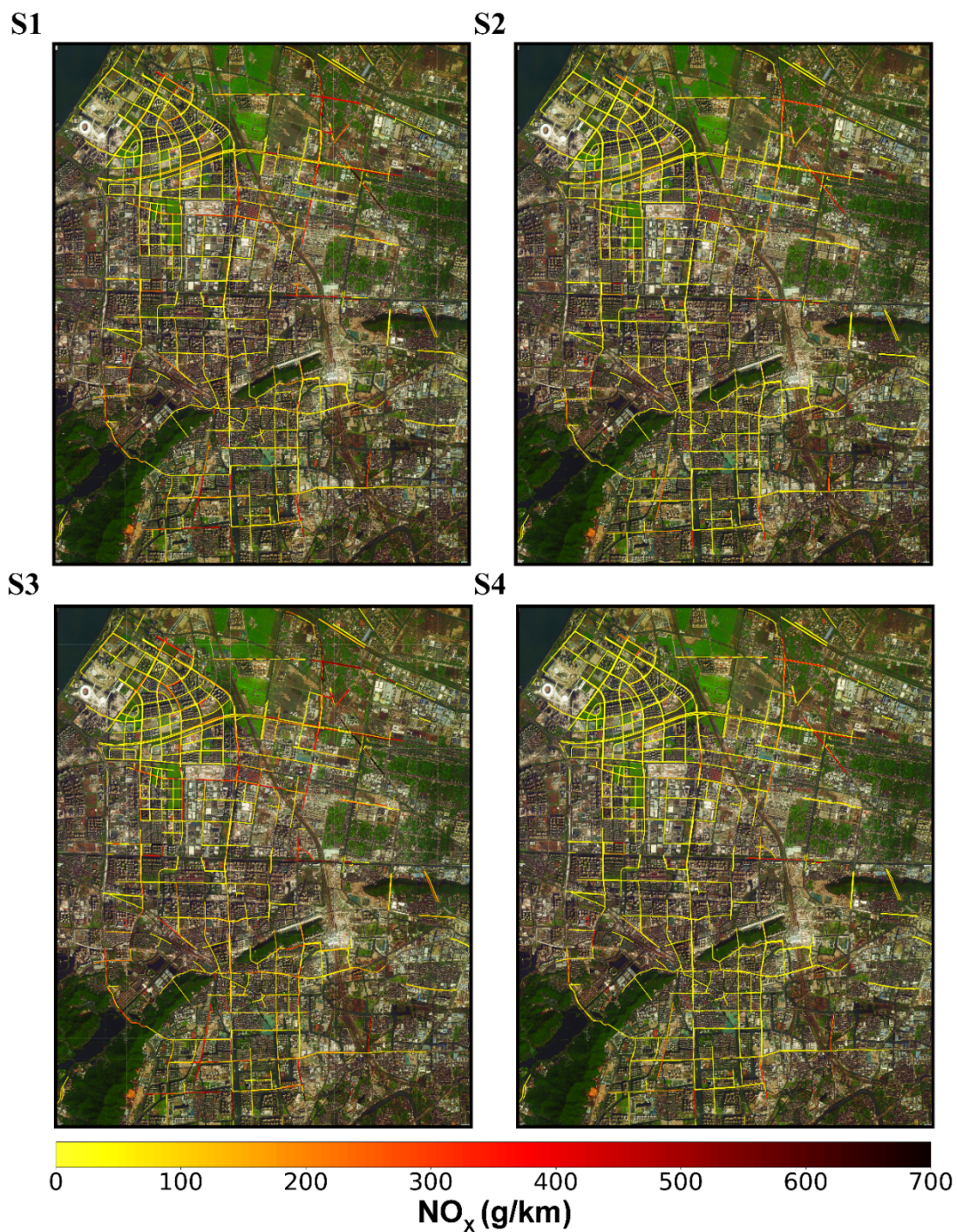
605



610

**Figure 6. Decay of on-road vehicle emissions, traffic fluxes, and vehicle categories from indicative hotspots outwards on weekdays. (a ~ d)** Points denote the ratio of hourly average emissions ( $\text{NO}_x$ , CO, HC, and  $\text{PM}_{2.5}$ ) over different road types at a given distance from hotspots to hourly average hotspot emissions. Error bars present standard deviations. An unconstrained three parameter exponential model reproduces the decay relationships with high fidelity. The isotropic parameter  $d$  reflected the distance to the hotspot cores ( $m$ ); the background parameter  $\alpha$  represented the background emissions far from the hotspots ( $d \rightarrow 1000\text{m}$ ); the parameter  $\beta$  represented the emission increment resulting from proximity to the hotspots; the decay parameter  $k$  governed the spatial scale over which emissions relaxed to  $\alpha$ . The subgraphs (e) and (f) are the same as (a) but for traffic fluxes and the vehicle category proportions, respectively.

615



620

**Figure 7.** Impacts of traffic control strategies (i.e., S1, ~ S4) on daily average on-road vehicle NO<sub>x</sub> emissions.

Map data © 2021, Gaode Map.



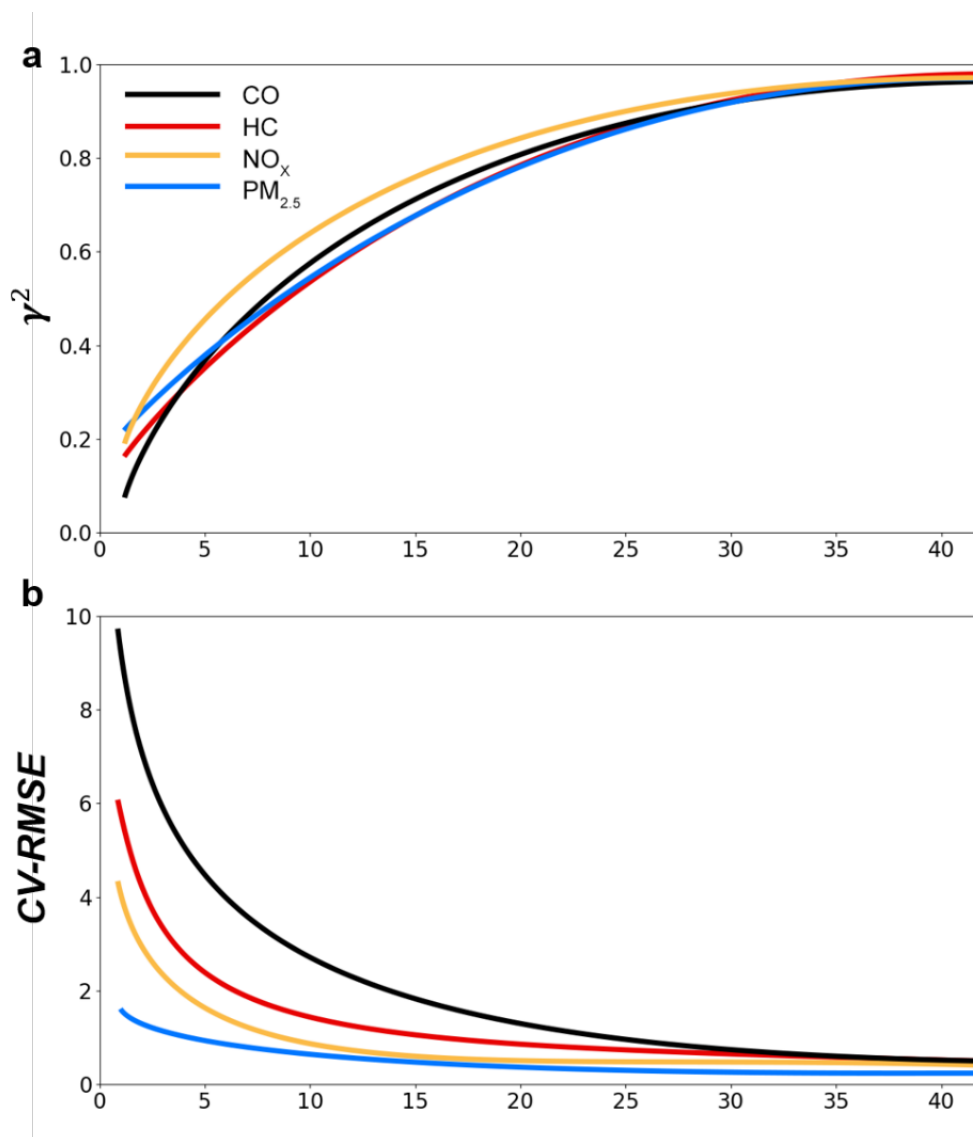


**Figure 8. Scaling analysis through systematic subsampling. (a)** Mean subsampled  $\gamma^2$  as a function of each road segment emissions relative to the full data set, plotted as function the number of unique weekdays for CO, HC,  $\text{NO}_x$ , and  $\text{PM}_{2.5}$ . **(b)** Mean subsampled coefficient of variation of root mean squared errors (**CV-RMSE**) versus the number of unique weekdays for CO, HC,  $\text{NO}_x$ , and  $\text{PM}_{2.5}$ .



**Table 1. Traffic control strategies.** The detailed rules are presented spatially and temporally.

Traffic control strategy	Time scale	Space scale	Vehicle category	Rule
S1	Morning and evening rush hours during from Monday to Friday	Arterial and residential roads	All	For each weekday (from Monday to Friday), vehicles with specific tail numbers of the license plates were prohibited on the arterial and residential roads during the morning and evening rush hours (from 7:00 to 9:00 and from 16:30 to 18:30, Local Time). The prohibited tail numbers were 1 and 9 on Monday, 2 and 8 on Tuesday, 3 and 7 on Wednesday, 4 and 6 on Thursday, and 5 and 0 on Friday.
S2	Morning and evening rush hours during from Monday to Friday	Arterial and residential roads	All	The even-odd rule for the license plates was adopted over the arterial and residential roads on weekdays.
S3	All day	Highways	HDVs and HDTs	Both local registered and non-registered trucks were strictly prohibited all day long over the highways.
S4	All day	All roads	All	All kinds of vehicles complied with the even-odd rule of the license plates over the entire District.